

Trajectory-aware Shifted State Space Models for Online Video Super-Resolution

Qiang Zhu¹, Xiandong Meng¹, Yuxuan Jiang², Fan Zhang², David Bull², Shuyuan Zhu³, Bing Zeng³

¹Pengcheng Labartory, ²University of Bristol, ³University of Electronic Science and Technology of China
 {zhuqiang,mengxd}@pcl.ac.cn, {yuxuan.jiang,fan.zhang,dave.bull}@bristol.ac.uk, {eeyzsy,eezeng}@uestc.edu.cn

Abstract

Online video super-resolution (VSR) is an important technique for many real-world video processing applications, which aims to restore the current high-resolution video frame based on temporally previous frames. Most of the existing online VSR methods solely employ one neighboring previous frame to achieve temporal alignment, which limits long-range temporal modeling of videos. Recently, state space models (SSMs) have been proposed with linear computational complexity and a global receptive field, which significantly improve computational efficiency and performance. In this context, this paper presents a novel online VSR method based on Trajectory-aware Shifted SSMs (TS-Mamba), leveraging both long-term trajectory modeling and low-complexity Mamba to achieve efficient spatio-temporal information aggregation. Specifically, TS-Mamba first constructs the trajectories within a video to select the most similar tokens from the previous frames. Then, a Trajectory-aware Shifted Mamba Aggregation (TSMA) module consisting of proposed shifted SSMs blocks is employed to aggregate the selected tokens. The shifted SSMs blocks are designed based on Hilbert scannings and corresponding shift operations to compensate for scanning losses and strengthen the spatial continuity of Mamba. Additionally, we propose a trajectory-aware loss function to supervise the trajectory generation, ensuring the accuracy of token selection when training our model. Extensive experiments on three widely used VSR test datasets demonstrate that compared with six online VSR benchmark models, our TS-Mamba achieves state-of-the-art performance in most cases and over 22.7% complexity reduction (in MACs). The source code for TS-Mamba will be available at <https://github.com>.

Introduction

Among various video super-resolution (VSR) application scenarios, online VSR has recently attracted significant interest due to the growing popularity of live video conferencing and live broadcasting applications (Fuoli et al. 2023; Xiao et al. 2023). In online VSR, the current high-resolution (HR) video frame is typically restored using only its low-resolution (LR) counterpart and previous frames. This is constrained by the requirements for low latency and low computational complexity inherent to these online real-time applications.

Copyright © 2026, Association for the Advancement of Artificial Intelligence (www.aaai.org). All rights reserved.

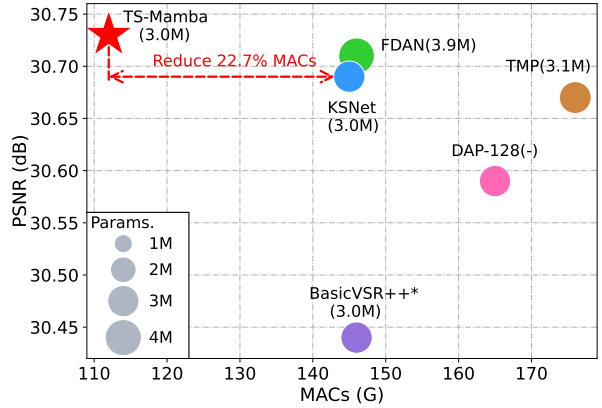


Figure 1: Comparison of existing online VSR methods with our TS-Mamba in terms of PSNR and MACs on REDS4 dataset. Our TS-Mamba outperforms these SOTA methods and significantly reduces complexity in terms of MACs.

In a VSR model, temporal alignment or aggregation is a core module employed to compensate for the information from neighboring frames before generating the current HR frame. Advanced temporal alignment or aggregation modules have been recently developed, which are based on deformable convolution networks (DCN) (Wang et al. 2019; Tian et al. 2020), flow-guided deformable alignment models (Chan et al. 2022; Zhu et al. 2024b), non-local attention mechanisms (Li et al. 2020; Yi et al. 2019) or Vision Transformer based spatio-temporal information aggregation (Liu et al. 2022a; Tang et al. 2023). Although they offer superior VSR performance, these methods are typically associated with high complexity and, therefore, are not ideal for online VSR.

To mitigate these limitations, recent online VSR methods have adopted more efficient temporal alignment modules, such as lightweight optical flow networks (Sajjadi, Vemulapalli, and Brown 2018; Xiao et al. 2023), deformable attention mechanisms (Fuoli et al. 2023; Yang et al. 2023), and temporal motion propagation modules (Zhang et al. 2024b). Despite their efficiency, these methods predominantly use short-term temporal information based on convolutional neural networks (CNN) — typically from a single previous frame, which restricts their ability to further enhance reconstruction quality. While incorporating long-term temporal alignment

can improve performance, it often introduces significant computational overhead, resulting in challenges for real-time or resource-constrained applications.

Recently, low-complexity state space models (SSMs) (Gu, Goel, and Ré 2021; Gu and Dao 2023) have been proposed with linear computational complexity and with relatively large receptive fields, which can potentially improve performance with limited complexity. Inspired by this, we propose a Trajectory-aware Shifted Mamba for online VSR, denoted as **TS-Mamba**, leveraging long-term trajectory modeling and low-complexity Mamba for achieving the token-level spatio-temporal aggregation. In TS-Mamba, trajectories within a video are first constructed for selecting the most similar tokens from the previous frames. A trajectory-aware shifted Mamba aggregation (TSMA) module is then employed, which consists of shifted SSMs blocks to aggregate the selected tokens. The shifted SSMs blocks are designed based on Hilbert scannings and four different shift operations to compensate for scanning losses and strengthen the spatial continuity of Mamba. Moreover, we propose a trajectory-aware loss function to supervise the trajectory generation, optimizing the accuracy of token selection when training our model. The proposed TS-Mamba model enables efficient long-term video modeling with significantly reduced computational complexity. The primary contributions are summarized as follows:

- TS-Mamba is the **first SSMs-based online VSR model**, which aggregates long-term spatio-temporal information from previous frames at the token level for restoring current HR frame. This is different from existing online VSR methods which typically use CNN-based temporal alignment to exploit temporal information from a single previous frame.
- This is also the **first time to introduce video trajectories** into Mamba to select the most similar tokens from previous frames and construct the new trajectory-aware shifted Mamba model for efficient token-level spatio-temporal information aggregation.
- The **novel shifted SSMs blocks** are designed based on four different shift operations and Hilbert scannings to effectively compensate for the intra-window and inter-window losses of Hilbert scannings and strengthen local spatial continuity of Mamba.

The proposed method has been benchmarked on three widely used test datasets and shows superior VSR performance with more than 22.7% computational complexity reduction in terms of MACs over five state-of-the-art (SOTA) online VSR methods (as shown in Figure 1).

Related Work

Video Super-Resolution

Video super-resolution (VSR) is a fundamental low-level vision task that aims to restore an HR video from its LR counterpart. Existing VSR methods are typically learning-based, utilizing various deep neural networks (Teed and Deng 2020; Zhu et al. 2019; Arnab et al. 2021; Ho et al. 2022). For example, optical flow-based methods (Chan et al. 2021; Liu et al. 2022b) explore the temporal motion between frames to

align them; deformable convolution networks (DCN)-based methods (Tian et al. 2020; Wang et al. 2019) learn the motion offsets between frames for feature alignment. Moreover, flow-guided deformable-based methods (Chan et al. 2022; Zhu et al. 2024b) combine optical flow and DCN to achieve better feature alignment. Non-local attention-based methods (Li et al. 2020; Yi et al. 2019) aggregate global information for feature aggregation. Vision Transformer-based methods (Liu et al. 2022a; Tang et al. 2023) aggregate long-term spatio-temporal information in video to restore SR frames. However, these methods are often associated with high complexity and are therefore not best suited for online VSR.

Online Video Super-Resolution

Due to the specific requirement of online applications, online VSR methods are expected to be lightweight and have low latency. Therefore, most existing online VSR methods have been proposed (Fuoli et al. 2023; Sajjadi, Vemulapalli, and Brown 2018; Xiao et al. 2023) with efficient feature alignment modules. For example, DAP (Fuoli et al. 2023) designed a deformable attention pyramid module to dynamically focus on the most salient locations between frames. FRVSR (Sajjadi, Vemulapalli, and Brown 2018) and CKBG (Xiao et al. 2023) utilized lightweight optical flow networks to estimate motion between frames and perform motion compensation. KSNet (Jin et al. 2023) proposed a kernel-split manner to reparameterize convolutional kernels on the high-value channel, enabling representation of dynamic information and reducing complexity along the channel dimension. FDAN (Yang et al. 2023) proposed a flow-guided deformable attention propagation module to efficiently exploit the temporal information between frames. TMP (Zhang et al. 2024b) employs an efficient temporal motion propagation method that leverages motion field continuity to achieve fast feature alignment. It is noted that, however, these online VSR methods are only based on one previous frame in feature alignment due to the complexity limitation, which hinders further improvement of VSR performance.

State Space Models

State space models (Gu, Goel, and Ré 2021; Gu and Dao 2023), e.g., Mamba, have been widely employed in vision tasks (Liu et al. 2024; Zhu et al. 2024a) due to their linear computational complexity and ability to model global dependencies. Mamba typically converts 2D images into 1D tokens through scanning (Qiao et al. 2024; Shi et al. 2025), resulting in spatial continuity loss inherent to images. More recently, advanced scanning techniques have emerged to address this issue, such as bidirectional scanning (Hu et al. 2024; Shi et al. 2025), cross scanning (Liu et al. 2024), continuous 2D scanning (Yang et al. 2024), and local scanning (Huang et al. 2024). To the best of our knowledge, the use of Mamba has not yet been investigated for the online video super-resolution task. Unlike existing Mamba-based works, we introduce sophisticated shift operations for Hilbert scannings to enhance the ability of Mamba to maintain local spatial continuity.

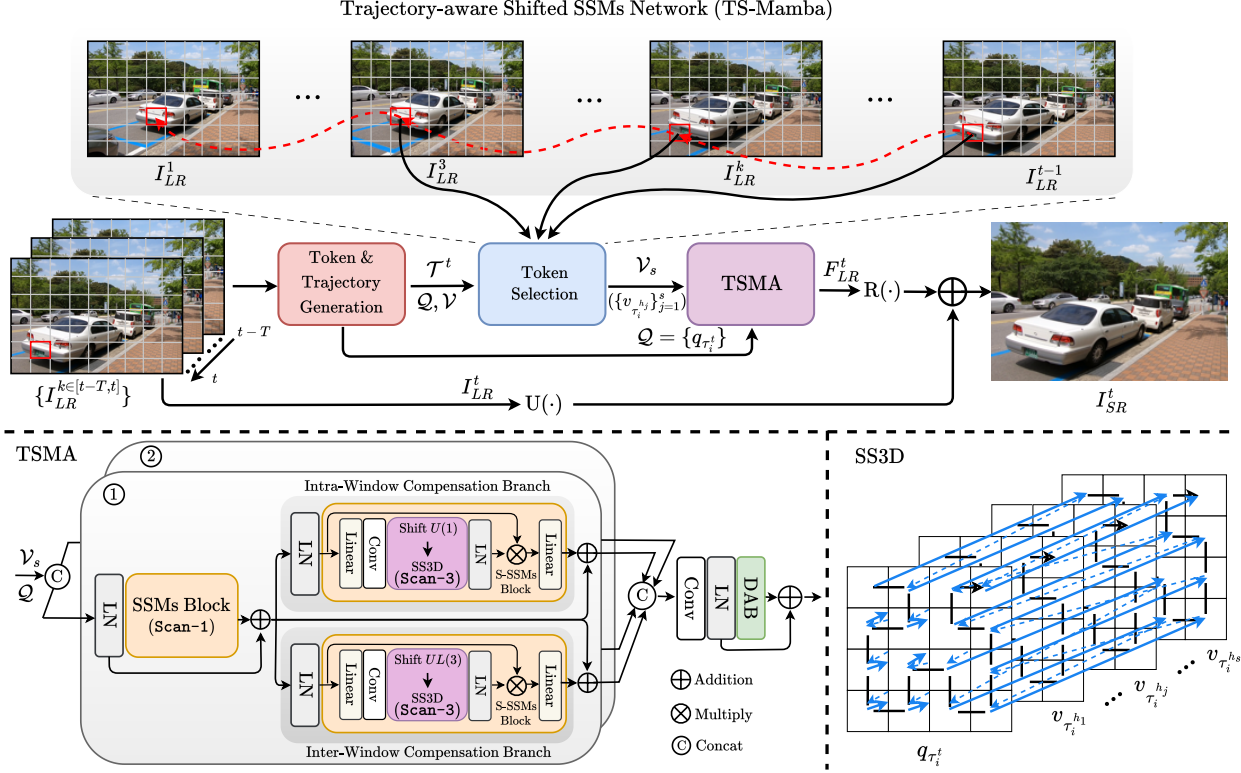


Figure 2: The architecture of the TS-Mamba network. Trajectories of videos are first generated and the similar tokens from previous frames are selected along trajectories. Then, the selected tokens alongside current frame token are fed into the trajectory-aware shifted Mamba aggregation (TSMA) module to achieve the long-term spatio-temporal information aggregation.

Methodology

In online video super-resolution, when reconstructing the t^{th} frame in a low-resolution video, we denote the current LR frame as I_{LR}^t and temporally previous LR frames as $\{I_{LR}^k, k \in [t-T, t-1]\}$. The proposed trajectory-aware shifted state space models, TS-Mamba, are illustrated in Figure 2. Here, all these LR video frames $\{I_{LR}^k, k \in [t-T, t]\}$ are first fed into the token and trajectory generation $G(\cdot)$ module to extract the current frame token Q and the tokens of previous LR frames V :

$$Q = G(I_{LR}^t) = \{q_i^t\}, i \in [1, N], \quad (1)$$

$$V = G(\{I_{LR}^k\}) = \{v_i^k\}, i \in [1, N], k \in [t-T, t-1], \quad (2)$$

where $G(\cdot)$ consists of a convolution layer and N_1 residual blocks to generate features and tokens from video frames, N is the token number, and T is the temporal window size.

Based on the generated tokens $\{q_i^t\}$, the trajectories \mathcal{T}^t of I_{LR}^t frame can be formulated as a set of trajectories,

$$\mathcal{T}^t = \{\tau_i^k = (x_i^k, y_i^k)\}, i \in [1, N], k \in [t-T, t], \quad (3)$$

where $x_i^k \in [1, H], y_i^k \in [1, W]$, and H and W represent the height and width of the feature (for LR frame), respectively. Each trajectory τ_i^k contains a sequence of coordinates $\{(x_i^k, y_i^k), i \in [1, N]\}$, and the end point of trajectory τ_i^t is associated with the coordinate (x_i^t, y_i^t) of token q_i^t .

We then select s the most similar tokens V_s along the trajectories and feed them into the proposed trajectory-aware shifted Mamba aggregation (TSMA) module alongside token Q to achieve spatio-temporal information aggregation:

$$F_{LR}^t = \text{TSMA}(Q, V_s). \quad (4)$$

Finally, the aggregated feature F_{LR}^t and the current LR frame I_{LR}^t are fed into the reconstruction network $R(\cdot)$ and the upsampling $U(\cdot)$ network, respectively, to produce the super-resolved frame I_{SR}^t :

$$I_{SR}^t = R(F_{LR}^t) + U(I_{LR}^t), \quad (5)$$

in which $R(\cdot)$ consists of two convolution layers, N_2 residual blocks, and a pixelshuffle layer. $U(\cdot)$ here represents the bicubic upsampling operation.

Token Selection

In order to select most similar tokens along trajectories, we first reformulate tokens Q, V associated with trajectories \mathcal{T}^t . Based on the formulation of the trajectories in Equation (3), tokens Q , and V can be formulated as:

$$\begin{aligned} Q &= \{q_{\tau_i^t}\}, i \in [1, N], \\ V &= \{v_{\tau_i^k}\}, i \in [1, N], k \in [t-T, t-1]. \end{aligned} \quad (6)$$

We compute the cosine similarity between the token Q , and tokens V to select s the most similar tokens along trajectories.

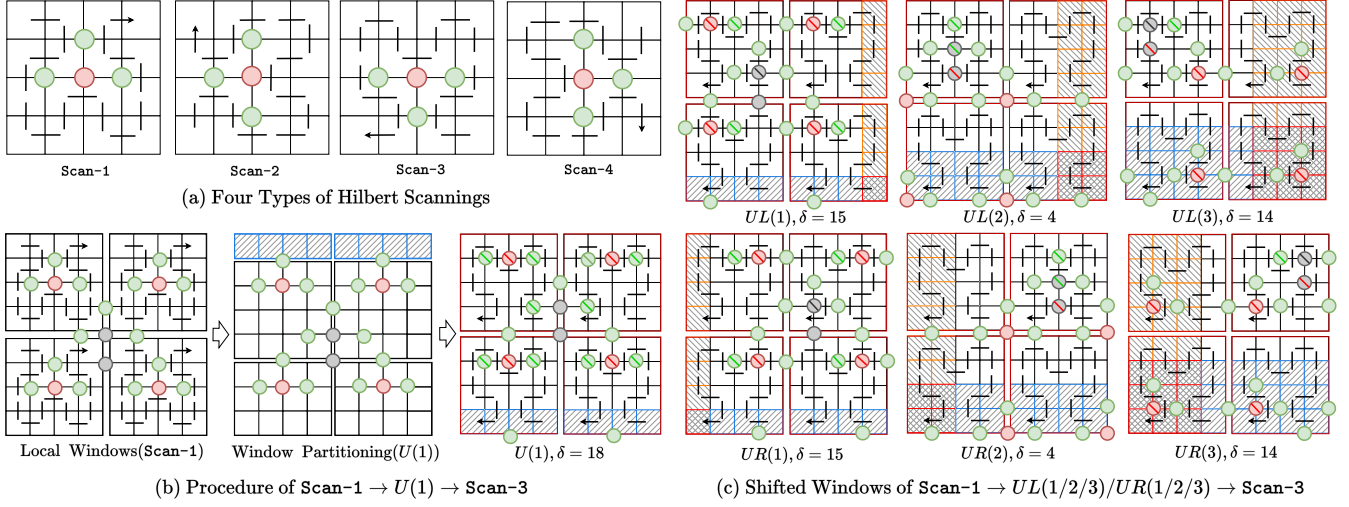


Figure 3: Illustration of Hilbert scannings and shifted windows generated by seven procedures. (a) Four types of Hilbert scannings. (b) The procedure of Scan-1 → U(1) → Scan-3 and elimination value δ . (c) Shifted windows and elimination values δ for procedures of Scan-1 → UL(1/2/3)/UR(1/2/3) → Scan-3, respectively.

The indices of the selected tokens and the selected tokens can be formulated as:

$$\begin{aligned} \{h_j\}_{j=1}^s &= \text{Top-k} \left\langle \frac{q_{\tau_i^t}}{\|q_{\tau_i^t}\|_2^2}, \frac{v_{\tau_i^k}}{\|v_{\tau_i^k}\|_2^2} \right\rangle, h_j \in [1, T-1], \\ \mathcal{V}_s &= \{v_{\tau_i^{h_j}}\}_{j=1}^s, i \in [1, N]. \end{aligned} \quad (7)$$

Thus, the process of the TS-Mamba network is described as:

$$\begin{aligned} I_{SR}^t &= \text{TS-Mamba}(\mathcal{Q}, \mathcal{V}, \mathcal{T}^t) \\ &= R(\text{TSMA}(q_{\tau_i^t}, \{v_{\tau_i^{h_j}}\}_{j=1}^s)) + U(I_{LR}^t). \end{aligned} \quad (8)$$

Trajectory-aware Shifted Mamba Aggregation

Mamba networks are typically used to convert 2D images into 1D tokens via scanning, resulting in spatial continuity losses inherent to the images. Existing works (Zhang et al. 2024a; Xiao and Wang 2025) do not analyze the degree of discontinuous regions but instead repeatedly use multiple scannings, making these methods hard to maintain the spatial continuity of the image and instead lead to greater complexity.

To address this issue, in this work, we first analyzed the spatial discontinuity in Hilbert scannings and then propose a trajectory-aware shifted Mamba aggregation (TSMA) module that combines a standard SSMs block and the proposed shifted SSMs (S-SSMs) blocks in the “Scan-Shift-Scan” manner to compensate for the intra-window and inter-window losses of Hilbert scannings. As illustrated in Figure 2, in the TSMA module, token \mathcal{Q} and selected tokens \mathcal{V}_s are first concatenated along the channel dimension and fed into two paths in a specific “Scan-Shift-Scan” manner, i.e., ① or ②, each of which consists of a standard SSMs block and two parallel S-SSMs blocks to compensate for the losses according to the scanning of the standard SSMs block. The output of each path is concatenated and then aggregated by a convolution layer

and a deformable attention block (DAB) (Xia et al. 2022) to obtain the output feature. Each SSMs/S-SSMs block and DAB is preceded by layer normalization (LN) and is followed by a residual connection. In each SSMs/S-SSMs block, the trajectory-aware tokens are scanned based on spatial Hilbert selective scannings along the temporal dimension (SS3D) to capture long-term spatio-temporal characteristics.

Discontinuity for Hilbert Scanning

To evaluate the spatial discontinuity of Hilbert scannings in local windows, we define the discontinuity degree D_d as follows. If the four adjacent areas are successively scanned, the region consisting of these four scanned areas is considered as continuous ($D_d = 0$); otherwise, the discontinuity degree D_d equals the number of areas that are not successively scanned. For a region consisting of four adjacent areas, the range of discontinuity degree is $D_d \in \{0, 1, 2, 3\}$. This is illustrated in Figure 3 (a), where four typical Hilbert scannings, i.e., Scan-1, Scan-2, Scan-3 and Scan-4 are shown on a 4x4 grid. Here the region with $D_d = 1$ is marked by a green circle and the region with $D_d = 2$ is marked by a red circle.

Moreover, we extend the general case to that based on the 8x8 grid to further discuss the discontinuity degrees. An 8x8 region is partitioned into four 4x4 local regions and we illustrate the discontinuity degree D_d within and between local windows under Scan-1 in Figure 3 (b). It can be observed that both intra-window discontinuity and inter-window discontinuity exist. In particular, due to the nature of Hilbert scanning, the central region between windows is widely spaced (the inter-window discontinuity), resulting in inter-level gaps. Here, the discontinuity degree D_d equals 3 - we mark this region with a gray circle in Figure 3 (b).

Shifted SSMs Block

To eliminate the discontinuity of Hilbert scannings, we propose the “Scan-Shift-Scan” manner that combines window

shifting with specific Hilbert scannings to strengthen the continuity of SSMs. The shifting can be defined based on the shift direction and shift position, e.g., Up 1 position ($U(1)$), Up Left 1 position ($UL(1)$) and Down Right 2 position ($DR(2)$). Our “Scan-Shift-Scan” manner is designed based on the four Hilbert scannings (shown in Figure 3 (a)) and these window shifting processes. As shown in Figure 3 (b), we illustrate the procedure of $\text{Scan-1} \rightarrow U(1) \rightarrow \text{Scan-3}$ as an example. The local windows are first partitioned by $U(1)$ shift operation and then cyclic fed as the shifted windows. It can be inferred that the second scanning (Scan-3) on the shifted window can eliminate the discontinuity of first scanning (Scan-1).

To evaluate the discontinuity elimination, we set three symbols and define an elimination value δ to mark and calculate the elimination. Specifically, we use green “\”, red “\”, and gray “\” on the circle for representation that eliminates 1, 2, and 3 discontinuity degrees, respectively, in Figure 3 (b)-(c). The elimination value δ is calculated by summing the eliminated discontinuity degrees that consist of intra-window discontinuity elimination and inter-window discontinuity elimination, i.e., $\delta = \delta_{\text{intra}} + \delta_{\text{inter}}$. We have investigated many combinations of shift operations and scannings, and illustrate the representative shifted windows generated by six shift operations, i.e., $UL(1)$, $UL(2)$, $UL(3)$, and $UR(1)$, $UR(2)$, $UR(3)$, under the first scanning (Scan-1) and second scanning (Scan-3) in Figure 3 (c). It can be inferred from Figure 3 (b)-(c) that the procedure of $\text{Scan-1} \rightarrow U(1) \rightarrow \text{Scan-3}$ achieves the best elimination ($\delta=18$) under the first scanning is Scan-1. This procedure achieves the best intra-window discontinuity elimination ($\delta_{\text{intra}}=18$) but doesn’t eliminate inter-window discontinuity ($\delta_{\text{inter}}=0$). We can infer that the other three procedures can also achieve the best elimination: $\text{Scan-2} \rightarrow L(1) \rightarrow \text{Scan-4}$, $\text{Scan-3} \rightarrow D(1) \rightarrow \text{Scan-1}$, $\text{Scan-4} \rightarrow R(1) \rightarrow \text{Scan-2}$. Moreover, the procedure of $\text{Scan-1} \rightarrow UL(3)/UR(3) \rightarrow \text{Scan-3}$ has the best inter-window discontinuity elimination ($\delta_{\text{inter}}=6$) but worse than the procedure of $\text{Scan-1} \rightarrow U(1) \rightarrow \text{Scan-3}$ for intra-window discontinuity elimination ($\delta_{\text{inter}}=8$). UL and UR shift operations exhibit symmetry under the first scanning Scan-1 and the second scanning Scan-3 when the same shift positions. Different combinations of shift operations and scannings can bring significant different elimination performance (more detail in our supplementary).

Based on these observations, we elaborately select shift operations and Hilbert scannings to construct two S-SSMs blocks in parallel branches, i.e., intra-window compensation branch (IntraWCB) and inter-window compensation branch (InterWCB), to eliminate corresponding discontinuities. As illustrated in Figure 2, we set two procedures for the parallel SSMs blocks to construct our TSMA module: ①: $\text{Scan-1} \rightarrow U(1) + UL(3) \rightarrow \text{Scan-3}$; ②: $\text{Scan-2} \rightarrow L(1) + LU(3) \rightarrow \text{Scan-4}$ to achieve sufficient elimination of discontinuity.

Selective Scanning along Temporal Dimension

To achieve temporal token aggregation, we implement spatial Hilbert-based selective scanning along the temporal dimension, i.e., SS3D. As shown in Figure 2, we showcase the

SS3D processing with Scan-1. The current token $\{q_{\tau_i^t}\}$ and selected tokens $\{v_{\tau_i^h j}\}_{j=1}^s$ are scanned to convert spatio-temporal neighboring pixels into a 1D token sequence. Each token sequence undergoes selective scanning based on the local windows. This process interweaves selected tokens with current tokens, enabling information to interact across spatial and temporal dimensions to capture long-term spatio-temporal characteristics. By scanning spatio-temporally adjacent pixels, SS3D preserves local spatial information and progressively captures global temporal patterns.

Loss Function

We adopt Charbonnier loss (Lai et al. 2018) as the spatial loss function to supervise the SR frame generation:

$$\mathcal{L}_{\text{spa}} = \sqrt{\|I_{HR}^t - I_{SR}^t\|^2 + \epsilon^2}, \quad (9)$$

in which I_{HR}^t is the HR frame and the ϵ is set to 1×10^{-4} .

To supervise the trajectory generation for ensuring the accuracy of token selection, we first employ the formulation of trajectories of LR video in Equation (3) to generate trajectories of HR video:

$$\mathcal{T}_{HR}^t = \left\{ \tau_{i(HR)}^k = (x_i^k, y_i^k) \right\}, i \in [1, M], k \in [t - T, t]. \quad (10)$$

Based on this, we propose our trajectory-aware loss function:

$$\mathcal{L}_{trj} = \|\mathcal{T}^t - ((\mathcal{T}_{HR}^t) \downarrow \hat{s}) / \hat{s}\|, \quad (11)$$

where $\downarrow \hat{s}$ is the downsampling operation with scale factor \hat{s} that subsamples every \hat{s} coordinate to LR size.

Overall, the total loss is:

$$\mathcal{L}_{total} = \mathcal{L}_{spa} + \lambda \mathcal{L}_{trj}, \quad (12)$$

in which the hyperparameter λ is set to 0.1.

Experiments

Experimental Settings

Following the previous online VSR research (Jin et al. 2023; Zhang et al. 2024b), we use REDS (Nah et al. 2019), and Vimeo-90K (Xue et al. 2019) as training datasets. REDS4 is used for evaluating the models trained on the REDS dataset, while Vimeo-90K-T and Vid4 (Liu and Sun 2013) are utilized for benchmarking the models trained on the Vimeo-90K dataset. Two degradations, BI (bicubic) and blur degradation (BD), are used to perform downsampling and the downsampling factor is set to $\hat{s} = 4$. For BI downsampling, the HR frame is downsampled by a bicubic filter. For BD downsampling, the HR frame is first blurred by a Gaussian filter with standard deviation $\sigma = 1.6$, and then the blurred frame is subsampled for every \hat{s} pixels to generate the LR frame. PSNR and SSIM are adopted as performance evaluation metrics. Runtime (Run.), FPS (frames per second), MACs, and parameters (Params.) are computed on an LR frame of size 180×320 to evaluate the model complexity and speed.

In the experiments, the numbers of residual blocks N_1 and N_2 are set to 2 and 13, respectively. The token size is 4×4 and the window size is 8×8 . The selected token

Category	Methods	Support Frame	R-T. (ms)	Run. (ms)	FPS↑ (1/s)	MACs. (G)	Params. (M)	BI degradation		BD degradation	
								REDS4(RGB)↑ (PSNR/SSIM)	Vid4(Y)↑ (PSNR/SSIM)	Vimeo-90K-T(Y)↑ (PSNR/SSIM)	Vid4(Y)↑ (PSNR/SSIM)
Bidirectional	BasicVSR (Chan et al. 2021)	P+F	X	63	15.9	397	6.3	31.42/0.8909	27.24/0.8251	37.53/0.9498	27.96/0.8553
	IconVSR (Chan et al. 2021)	P+F	X	70	14.3	452	8.7	31.67/0.8948	27.39/0.8279	37.84/0.9524	28.04/0.8570
	BasicVSR++ (Chan et al. 2022)	P+F	X	77	13.0	418	7.3	32.39/0.9069	27.79/0.8400	38.21/0.9550	29.04/0.8753
	SSL-bi (Chan et al. 2021)	P+F	X	24	41.7	92	1.0	31.06/0.8933	27.15/0.8208	37.06/0.9458	27.56/0.8431
Online VSR	Bicubic	N	✓	-	-	-	-	26.14/0.7292	23.78/0.6347	31.30/0.8687	21.80/0.5246
	RRN (Chan et al. 2021)	P	✓	34	29.4	193	3.4	28.82/0.8234	25.85/0.7660	36.69/0.9432	27.69/0.8488
	BasicVSR++*	P	✓	40	25.0	146	3.0	30.44/0.8686	27.06/0.8173	37.11/0.9464	27.49/0.8426
	DAP-128 (Fuoli et al. 2023)	P	✓	38	26.3	165	-	30.59/0.8703	-	37.29/0.9476	-
	FDAN (Yang et al. 2023)	P	✓	34	29.4	146	3.9	<u>30.71</u> /0.8723	<u>27.14</u> /0.8206 [†]	37.36/0.9483[†]	27.76/0.8471
	KSNet (Jin et al. 2023)	P	✓	31	32.3	<u>145</u>	3.0	30.69/0.8724	27.14/0.8208	<u>37.34/0.9490</u>	27.63/0.8444 [†]
	TMP (Zhang et al. 2024b)	P	✓	25	40.1	176	<u>3.1</u>	30.67/0.8710	27.10/0.8167	37.33/0.9481	27.61/0.8428
TS-Mamba (ours)		P	✓	<u>29</u>	<u>33.5</u>	112	3.0	30.73/0.8727	27.17/0.8209	37.36/0.9482	<u>27.70/0.8473</u>

Table 1: Comparison with state-of-the-art online VSR methods. The runtime, FPS, parameters, and PSNR(dB)/SSIM are reported on three benchmarks with BI and BD degradations.

number s is set as 3. Random flips, rotations, and temporal inversion operations are performed for data augmentation. Adam optimizer (Kingma 2014), and Cosine Annealing scheme (Loshchilov and Hutter 2016) are used during network training. The HR patch size is 256×256 and the batch size is 8. The total number of iterations is 600K. The proposed method is implemented on the PyTorch platform with two NVIDIA GeForce RTX 3090 GPUs. Following (Liu et al. 2022a), a lightweight optical flow network (Kong, Shen, and Yang 2021) is adopted to update trajectories. The temporal window size T is set as 15 based on (Zhang et al. 2024b) when training on REDS (Nah et al. 2019). For the Vimeo-90K (Xue et al. 2019) dataset, the original sequence is temporally flipped to obtain a 14-frame sequence.

We compare our approach with five SOTA online VSR methods, including RRN (Isobe et al. 2020), DAP-128 (Fuoli et al. 2023), FDAN (Yang et al. 2023), KSNet (Jin et al. 2023), and TMP (Zhang et al. 2024b), and four bidirectional propagation VSR methods, BasicVSR (Chan et al. 2021), IconVSR (Chan et al. 2021), BasicVSR++ (Chan et al. 2022), and SSL (Xia et al. 2023)). Additionally, we implemented another method, i.e., “BasicVSR++*”, by removing the backward propagation branch of BasicVSR++ and reducing its model size for online VSR application. We use “P”, “F” and “N” to represent those with the previous support frames, future support frames and no support frames.

Overall Performance

As shown in Table 1, the quantitative results demonstrate the superior performance of the proposed method over other online VSR models in terms of PSNR and SSIM. We also supplement the results of FDAN and KSNet models on Vid4 and Vimeo-90K-T datasets based on their released pre-trained models and source codes for a comprehensive comparison. These results are reported in Table 1 with “ † ”. Figure 4 presents qualitative comparisons, from which we can ob-

Models	PSNR/SSIM	Params.	Run.	MACs
(v1.1) w/o Trajectory	30.45/0.8678	1.7	20	84
(v1.2) w/o \mathcal{L}_{trj}	30.70/0.8721	3.0	29	112
(v1.3) w/o IntraWCB	30.58/0.8702	2.8	25	97
(v1.4) w/o InterWCB	30.61/0.8706	2.8	25	97
(v1.5) w/o IntraWCB+InterWCB	30.52/0.8689	2.4	21	85
(v1.6) w/o $U(1)/D(1)$	30.65/0.8710	3.0	27	112
(v1.7) w/o $UL(3)/DL(3)$	30.67/0.8714	3.0	27	112
(v1.8) w/o (v1.6) + (v1.7)	30.61/0.8702	3.0	25	111
TS-Mamba (ours)	30.73/0.8727	3.0	29	112

Table 2: Results of the ablation study.

serve that our method shows better visual quality than other online VSR methods for both BI and BD degradations.

Following (Fuoli et al. 2023; Zhang et al. 2024b), VSR methods that can process 720p (1280×720) videos in at least 24 in terms of FPS are recognized as real-time (R-T.) methods (Fuoli et al. 2023), and we have labelled all the tested methods in Table 1 according to their runtime. It is noted that our TS-Mamba model achieves the second fastest inference speed among all online VSR methods. TMP is the one with the fastest runtime as it was implemented with the CUDA accelerator (high MACs but low runtime) while TS-Mamba is not. Moreover, TS-Mamba also offers a significant reduction in terms of MACs (about 36.3%) and a marginal reduction in parameter numbers compared to TMP, as shown in Figure 1.

Ablation Study

To further verify the effectiveness of our contributions, we have conducted ablation studies on the REDS4 dataset.

We first confirmed the contribution of two trajectory-aware designs, i.e., trajectory generation and trajectory-aware loss,

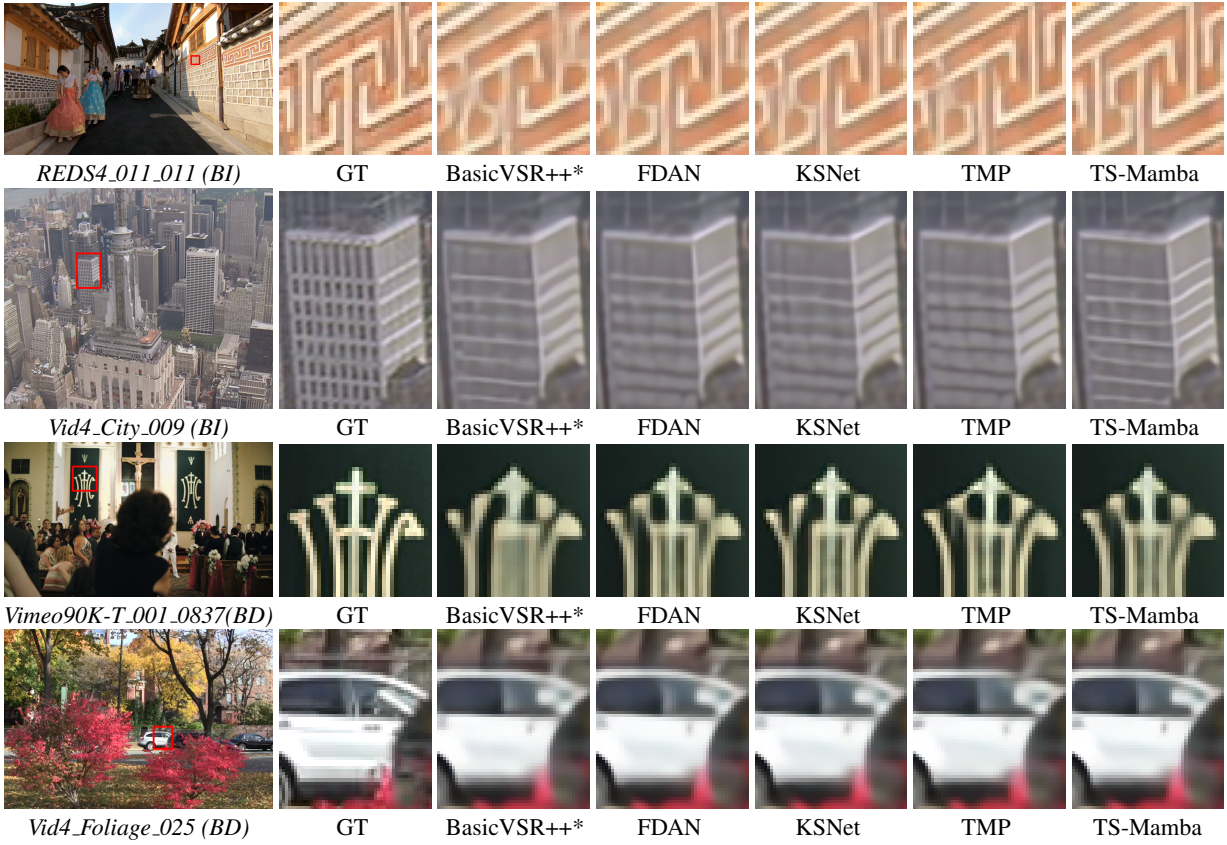


Figure 4: Visual comparison results on BI degradation (REDS4, Vid4) and BD degradation (Vimeo-90K-T, Vid4).

by creating the following variants. (v1.1) *w/o* Trajectory - $G(\cdot)$ and Token Selection module were removed from TS-Mamba; (v1.2) *w/o* \mathcal{L}_{trj} - the trajectory-aware loss function was removed when training the TS-Mamba model. We further verified our proposed TSMA module in terms of compensation branches and shift operations, by obtaining (v1.3) *w/o* IntraWCB and (v1.4) *w/o* InterWCB - IntraWCB and InterWCB were removed from TSMA module, respectively; (v1.5) *w/o* IntraWCB + InterWCB - both IntraWCB and InterWCB were removed from the TSMA module. We also tested the adopted shift operations in compensation branches, and implemented (v1.6) *w/o* $U(1)/L(1)$ - the $U(1)/L(1)$ shift operations were removed in IntraWCB, (v1.7) *w/o* $UL(3)/LU(3)$ - the $UL(3)/LU(3)$ shift operations were removed in InterWCB and (v1.8) *w/o* (v1.6)+(v1.7) - all the shift operations were removed in TSMA module. As shown in Table 2, the performance of all these variants is evidently lower than that of the full TS-Mamba, which fully confirmed the effectiveness of each key component in our design.

To confirm the value of the token number s in our TS-Mamba, we tested different s values with our TS-Mamba model, and presented the results in Table 3. It is noted that as s increases, the VSR performance improves, but with higher model complexity. When $s = 4$, it is difficult to obviously improve VSR performance. To trade off between complexity and performance, we set $s = 3$ in this work.

s	PSNR/SSIM	Params.	Run.	MACs
1	30.64/0.8712	2.8	25	96
2	30.68/0.8720	2.9	27	104
3	30.73/0.8727	3.0	29	112
4	30.74/0.8727	3.1	31	120

Table 3: Ablation study of selected token number s .

Conclusion

In this paper, we proposed a Trajectory-aware Shifted SSMs (**TS-Mamba**) for online VSR, leveraging long-term trajectory modeling and low-complexity Mamba to achieve efficient spatio-temporal information aggregation. In TS-Mamba, trajectories in a video are first constructed to select the most similar tokens from the previous frames. A trajectory-aware shifted Mamba aggregation module is then employed, which consists of shifted SSMs blocks to aggregate the selected tokens. The shifted SSMs blocks are designed based on Hilbert scanings and shift operations to compensate for the scanning losses and strengthen the spatial continuity of Mamba. Moreover, a trajectory-aware loss function is proposed to supervise the trajectory generation, optimizing the accuracy of token selection when training our model. Extensive experiments on three widely used VSR benchmarks have demonstrated the effectiveness and efficiency of our method.

References

Arnab, A.; Dehghani, M.; Heigold, G.; Sun, C.; Lučić, M.; and Schmid, C. 2021. Vivit: A video vision transformer. In *Proceedings of the IEEE/CVF International Conference on Computer Vision*, 6836–6846.

Chan, K. C.; Wang, X.; Yu, K.; Dong, C.; and Loy, C. C. 2021. Basicvssr: The search for essential components in video super-resolution and beyond. In *Proceedings of the IEEE/CVF Conference on Computer Vision and Pattern Recognition*, 4947–4956.

Chan, K. C.; Zhou, S.; Xu, X.; and Loy, C. C. 2022. Basicvssr++: Improving video super-resolution with enhanced propagation and alignment. In *Proceedings of the IEEE/CVF Conference on Computer Vision and Pattern Recognition*, 5972–5981.

Fuoli, D.; Danelljan, M.; Timofte, R.; and Van Gool, L. 2023. Fast online video super-resolution with deformable attention pyramid. In *Proceedings of the IEEE/CVF Winter Conference on Applications of Computer Vision*, 1735–1744.

Gu, A.; and Dao, T. 2023. Mamba: Linear-time sequence modeling with selective state spaces. *arXiv preprint arXiv:2312.00752*.

Gu, A.; Goel, K.; and Ré, C. 2021. Efficiently modeling long sequences with structured state spaces. *arXiv preprint arXiv:2111.00396*.

Ho, J.; Salimans, T.; Gritsenko, A.; Chan, W.; Norouzi, M.; and Fleet, D. J. 2022. Video diffusion models. *Advances in Neural Information Processing Systems*, 35: 8633–8646.

Hu, V. T.; Baumann, S. A.; Gui, M.; Grebenkova, O.; Ma, P.; Fischer, J.; and Ommer, B. 2024. Zigma: A dit-style zigzag mamba diffusion model. In *Proceedings of the European Conference on Computer Vision*, 148–166. Springer.

Huang, T.; Pei, X.; You, S.; Wang, F.; Qian, C.; and Xu, C. 2024. Localmamba: Visual state space model with windowed selective scan. In *Proceedings of the European Conference on Computer Vision*, 12–22. Springer.

Isobe, T.; Zhu, F.; Jia, X.; and Wang, S. 2020. Revisiting temporal modeling for video super-resolution. *arXiv preprint arXiv:2008.05765*.

Jin, S.; Liu, M.; Yao, C.; Lin, C.; and Zhao, Y. 2023. Kernel dimension matters: To activate available kernels for real-time video super-resolution. In *Proceedings of the 31st ACM International Conference on Multimedia*, 8617–8625.

Kingma, D. P. 2014. Adam: A method for stochastic optimization. *arXiv preprint arXiv:1412.6980*.

Kong, L.; Shen, C.; and Yang, J. 2021. Fastflownet: A lightweight network for fast optical flow estimation. In *2021 IEEE International Conference on Robotics and Automation*, 10310–10316. IEEE.

Lai, W.-S.; Huang, J.-B.; Ahuja, N.; and Yang, M.-H. 2018. Fast and accurate image super-resolution with deep laplacian pyramid networks. *IEEE Transactions on Pattern Analysis and Machine Intelligence*, 41(11): 2599–2613.

Li, W.; Tao, X.; Guo, T.; Qi, L.; Lu, J.; and Jia, J. 2020. Mucan: Multi-correspondence aggregation network for video super-resolution. In *Proceedings of the European Conference on Computer Vision*, 335–351. Springer.

Liu, C.; and Sun, D. 2013. On Bayesian adaptive video super resolution. *IEEE Transactions on Pattern Analysis and Machine Intelligence*, 36(2): 346–360.

Liu, C.; Yang, H.; Fu, J.; and Qian, X. 2022a. Learning trajectory-aware transformer for video super-resolution. In *Proceedings of the IEEE/CVF Conference on Computer Vision and Pattern Recognition*, 5687–5696.

Liu, M.; Jin, S.; Yao, C.; Lin, C.; and Zhao, Y. 2022b. Temporal consistency learning of inter-frames for video super-resolution. *IEEE Transactions on Circuits and Systems for Video Technology*, 33(4): 1507–1520.

Liu, Y.; Tian, Y.; Zhao, Y.; Yu, H.; Xie, L.; Wang, Y.; Ye, Q.; Jiao, J.; and Liu, Y. 2024. Vmamba: Visual state space model. *Advances in Neural Information Processing Systems*, 37: 103031–103063.

Loshchilov, I.; and Hutter, F. 2016. Sgdr: Stochastic gradient descent with warm restarts. *arXiv preprint arXiv:1608.03983*.

Nah, S.; Baik, S.; Hong, S.; Moon, G.; Son, S.; Timofte, R.; and Mu Lee, K. 2019. Ntire 2019 challenge on video deblurring and super-resolution: Dataset and study. In *Proceedings of the IEEE/CVF Conference on Computer Vision and Pattern Recognition workshops*, 1996–2005.

Qiao, Y.; Yu, Z.; Guo, L.; Chen, S.; Zhao, Z.; Sun, M.; Wu, Q.; and Liu, J. 2024. Vl-mamba: Exploring state space models for multimodal learning. *arXiv preprint arXiv:2403.13600*.

Sajjadi, M. S.; Vemulapalli, R.; and Brown, M. 2018. Frame-recurrent video super-resolution. In *Proceedings of the IEEE Conference on Computer Vision and Pattern Recognition*, 6626–6634.

Shi, Y.; Xia, B.; Jin, X.; Wang, X.; Zhao, T.; Xia, X.; Xiao, X.; and Yang, W. 2025. Vmambair: Visual state space model for image restoration. *IEEE Transactions on Circuits and Systems for Video Technology*.

Tang, J.; Lu, C.; Liu, Z.; Li, J.; Dai, H.; and Ding, Y. 2023. CTVSR: Collaborative spatial-temporal transformer for video super-resolution. *IEEE Transactions on Circuits and Systems for Video Technology*.

Teed, Z.; and Deng, J. 2020. Raft: Recurrent all-pairs field transforms for optical flow. In *Proceedings of the European Conference on Computer Vision*, 402–419. Springer.

Tian, Y.; Zhang, Y.; Fu, Y.; and Xu, C. 2020. Tdan: Temporally-deformable alignment network for video super-resolution. In *Proceedings of the IEEE/CVF Conference on Computer Vision and Pattern Recognition*, 3360–3369.

Wang, X.; Chan, K. C.; Yu, K.; Dong, C.; and Change Loy, C. 2019. Edvr: Video restoration with enhanced deformable convolutional networks. In *Proceedings of the IEEE/CVF Conference on Computer Vision and Pattern Recognition workshops*, 1954–1963.

Xia, B.; He, J.; Zhang, Y.; Wang, Y.; Tian, Y.; Yang, W.; and Van Gool, L. 2023. Structured sparsity learning for efficient video super-resolution. In *Proceedings of the IEEE/CVF Conference on Computer Vision and Pattern Recognition*, 22638–22647.

Xia, Z.; Pan, X.; Song, S.; Li, L. E.; and Huang, G. 2022. Vision transformer with deformable attention. In *Proceedings of the IEEE/CVF conference on computer vision and pattern recognition*, 4794–4803.

Xiao, J.; Jiang, X.; Zheng, N.; Yang, H.; Yang, Y.; Yang, Y.; Li, D.; and Lam, K.-M. 2023. Online video super-resolution with convolutional kernel bypass grafts. *IEEE Transactions on Multimedia*, 25: 8972–8987.

Xiao, Z.; and Wang, X. 2025. Event-based Video Super-Resolution via State Space Models. In *Proceedings of the Computer Vision and Pattern Recognition Conference*, 12564–12574.

Xue, T.; Chen, B.; Wu, J.; Wei, D.; and Freeman, W. T. 2019. Video enhancement with task-oriented flow. *International Journal of Computer Vision*, 127: 1106–1125.

Yang, C.; Chen, Z.; Espinosa, M.; Ericsson, L.; Wang, Z.; Liu, J.; and Crowley, E. J. 2024. Plainmamba: Improving non-hierarchical mamba in visual recognition. *arXiv preprint arXiv:2403.17695*.

Yang, X.; Zhang, X.; Zhang, L.; and Zhang, L. 2023. Flow-guided deformable attention network for fast online video super-resolution. In *2023 IEEE International Conference on Image Processing*, 390–394. IEEE.

Yi, P.; Wang, Z.; Jiang, K.; Jiang, J.; and Ma, J. 2019. Progressive fusion video super-resolution network via exploiting non-local spatio-temporal correlations. In *Proceedings of the IEEE/CVF International Conference on Computer Vision*, 3106–3115.

Zhang, G.; Liu, C.; Cui, Y.; Zhao, X.; Ma, K.; and Wang, L. 2024a. Vfimamba: Video frame interpolation with state space models. *Advances in Neural Information Processing Systems*, 37: 107225–107248.

Zhang, Z.; Li, R.; Guo, S.; Cao, Y.; and Zhang, L. 2024b. Tmp: Temporal motion propagation for online video super-resolution. *IEEE Transactions on Image Processing*.

Zhu, L.; Liao, B.; Zhang, Q.; Wang, X.; Liu, W.; and Wang, X. 2024a. Vision mamba: Efficient visual representation learning with bidirectional state space model. In *International Conference on Machine Learning*, 62429–62442. PMLR.

Zhu, Q.; Chen, F.; Zhu, S.; Liu, Y.; Zhou, X.; Xiong, R.; and Zeng, B. 2024b. DVSRNet: Deep video super-resolution based on progressive deformable alignment and temporal-sparse enhancement. *IEEE Transactions on Neural Networks and Learning Systems*.

Zhu, X.; Hu, H.; Lin, S.; and Dai, J. 2019. Deformable convnets v2: More deformable, better results. In *Proceedings of the IEEE/CVF Conference on Computer Vision and Pattern Recognition*, 9308–9316.